Received: 3 September 2018 | Revised: 19 November 2018 | Accepted: 16 December 2018

DOI: 10.1111/cbdd.13473

RESEARCH ARTICLE

WILEY C&B DRUG DESIGN

# Pharmacophoric features for a very potent 5-spirofluorenehydantoin inhibitor of cancer efflux pump ABCB1, based on X-ray analysis

**Ewa Żesławska**[1] | **Annamária Kincses**[2] | **Gabriella Spengler**[2] | **Wojciech Nitek**[3] | **Waldemar Tejchman**[1] | **Jadwiga Handzlik**[4]

[1]Department of Chemistry, Institute of Biology, Pedagogical University of Cracow, Kraków, Poland

[2]Department of Medical Microbiology and Immunobiology, Faculty of Medicine, University of Szeged, Szeged, Hungary

[3]Faculty of Chemistry, Jagiellonian University, Kraków, Poland

[4]Department of Technology and Biotechnology of Drugs, Jagiellonian University Medical College, Kraków, Poland

**Correspondence**
Ewa Żesławska, Department of Chemistry, Institute of Biology, Pedagogical University of Cracow, Kraków, Poland.
Email: ewa.zeslawska@up.krakow.pl

**Funding information**
Pedagogical University of Cracow, Grant/Award Number: BS-465/G/2018; Polish Statutory Research Project, Grant/Award Number: K/ZDS/007886

**Abstract**

In order to extend knowledge about pharmacophoric features responsible for ABCB1 inhibitory properties of imidazolidin-2,4-dione derivatives, 1′-[4-(4-(o-methoxyphenyl)-piperazin-1-yl)butyl]-3′-methyl-spiro(fluoren-9,5′-imidazolidine)-2′,4′-dione (**3**) and its salt (**4**) with rhodanine-3-acetic acid (**RA**) were prepared and investigated by X-ray diffraction method, as well as their efflux modulating effects in cancer cells (mouse T-lymphoma), cytotoxic and antiproliferative activities were evaluated in vitro. The molecular geometry, intermolecular interactions, and crystal packing of base and acid forms of **3** were analyzed to see, if conformational changes influence the biological activities. The geometry of 2-methoxyphenylpiperazine and 5-spirofluorenehydantoin moieties was compared with other crystal structures containing these fragments. Our results indicated a very potent inhibitory action on ABCB1 pump, and significant cytotoxic and antiproliferative properties of **3** in T-lymphoma, even more potent in the case of multidrug resistance cells. Furthermore, the compound **3** converted into the salt **4** of inactive acid (**RA**) has maintained both, the efflux pump inhibitory and antiproliferative activities, showing strong synergism with doxorubicin. A comparison of geometry of **3** in both crystal structures (**3** and **4**) shows a significant difference in the arrangement of piperazine ring with respect to the aliphatic linker.

**KEYWORDS**

arylpiperazine derivative of hydantoin, crystal structure, efflux pump inhibitor, pharmacophor, rhodanine-3-acetic acid

## 1 | INTRODUCTION

Hydantoin (imidazolidin-2,4-dione) is an interesting heterocyclic core of a variety of biologically active compounds, including those present in pharmaceutical market, for example, anticonvulsant phenytoin (5,5-diphenylhydantoin) or nilutamide (5,5-dimethyl-3-(4-nitro-3-(trifluoromethyl) phenyl)imidazolidine-2,4-dione), useful in the treatment of prostate cancer (Raynaud, Bonne, Bouton, Lagace, & Labrie, 1979; Raynaud et al., 1984). Furthermore, the imidazolidine-2,4-dione is a grateful pattern for chemical modifications (at position 5 and at the nitrogen atoms in the position 1 and 3 susceptible for various alkylations), which can enrich this chemical structure to strengthen, extend, or profile its biological activity. Consequently, a vast number of previously obtained 5-aromatic hydantoin derivatives, with amine moieties at 1- or 3-positions, demonstrated wide spectrum of pharmacological properties, including the following: antimicrobial

(Szymańska & Kieć-Kononowicz, 2002; Szymańska, Kieć-Kononowicz, Białecka, & Kasprowicz, 2002), hypotensive, antiarrhythmic- or/and GPCR-agents actions (Handzlik et al., 2008, 2011). An increasing interest of potential usage of 5-, 1- and/or 3-substituted hydantoin derivatives in various aspects of cancer treatment has provided a series of active agents for the last decade. In this context, the 5-benzylidene-hydantoins inhibiting epidermal growth factor receptor (Carmi et al., 2006), active against prostate (Khanfar & El Sayed, 2010), or lung cancer (Cavazzoni et al., 2008) were described. In contrary, results of our previous studies indicated no anticancer activity, but a very high inhibitory potency against multidrug resistance (MDR) cancer efflux pump (ABCB1) for both, the 5-aryl and 5-arylidene, derivatives of hydantoin that also contained an arylpiperazine fragment at position 1 or 3 (Spengler et al., 2010, 2011; Żesławska et al., 2016). Especially, potent efflux pump inhibitory (EPI) action, found for the 5,5-diphenylhydantoin arylpiperazine derivatives containing rotable phenyl moieties (**BS-1**, Figure 1a), seemed to be a sufficient reason to investigate also their immobile analogues that were obtained by introduction of the spirofluorene moiety at position 5 of hydantoin. A comparable analysis of the MDR EPI properties, evaluated in cancer T-lymphoma cells for both spirofluorene and diphenyl 3-ester substituted analogues, indicated that spiro(fluoren-9,5′-imidazolidine)-2′,4′-dione derivatives (**1** and **2**, Figure 1b) are worthy of further and extended considerations in the search for effective "adjuvants," useful for future anticancer therapy.

Taking into account beneficial substituents at position 1 found for the previous potent hydantoin EPIs (**BS-1**, **LL-9**, Figure 1) (Spengler et al., 2010), we decided to investigate the 3-methyl- and 1-(2-alkoxyphenyl)piperazine derivatives in the next step.

In order to extend knowledge about this new chemical group of potential "adjuvants" for anticancer drugs, this study is focused on single and cooperative biological actions of one representative basic member and an appropriate acid, including a deeper insight into structural properties of each one and of their combination. In this context, we prepared 1′-[4-(4-(o-methoxyphenyl)-piperazin-1-yl)butyl]-3′-methyl-spiro(fluoren-9,5′-imidazolidine)-2′,4′-dione (**3**) and its salt (**4**) with rhodanine-3-acetic acid (**RA**; Figure 2) to determine their crystal and molecular structures, as well as to evaluate their efflux modulating effects in cancer cells (mouse T-lymphoma), cytotoxic and antiproliferative activities.

The crystal structure analysis of salts consisting of two organic compounds is very interesting, since it allows the examination of molecules conformations, especially the search for conformational changes of ionic molecules (Żesławska, Jacob, Sturzebecher, & Oleksyn, 2006; Żesławska, Nitek, & Handzlik, 2017; Żesławska, Nitek, Marona, & Waszkielewicz, 2018; Żesławska, Oleksyn, Fabre, & Benoit-Vical, 2014; Żesławska, Oleksyn, & Stadnicka, 2003; Żesławska, Sturzebecher, & Oleksyn, 2007). The preparation of multicomponent monocrystals suitable for X-ray analysis is a great challenge, but it is worth the effort due the deeper insight into the structural properties coming from X-ray analysis, which provides valuable information about possible conformational changes. The study of crystal structure of **4** gives a possibility to compare the conformational changes of **3** under an influence of the acid molecule (**RA**). We analyzed the molecular geometry, intermolecular interactions, and crystal packing of base and acid forms of **3** in order to know, if conformational changes influence the biological activities. We compared also geometries of **3** and **4** with crystal structures of other 5-spirofluorenehydantoin derivatives with determined biological activities toward their efflux modulating and cytotoxicity effects in cancer cells (mouse T-lymphoma) (Żesławska et al., 2016). Furthermore, we carried out a search of the Cambridge Structural Database (CSD, Version 5.39) (Groom, Bruno, Lightfoot, & Ward, 2016) for 2-methoxyphenylpiperazine

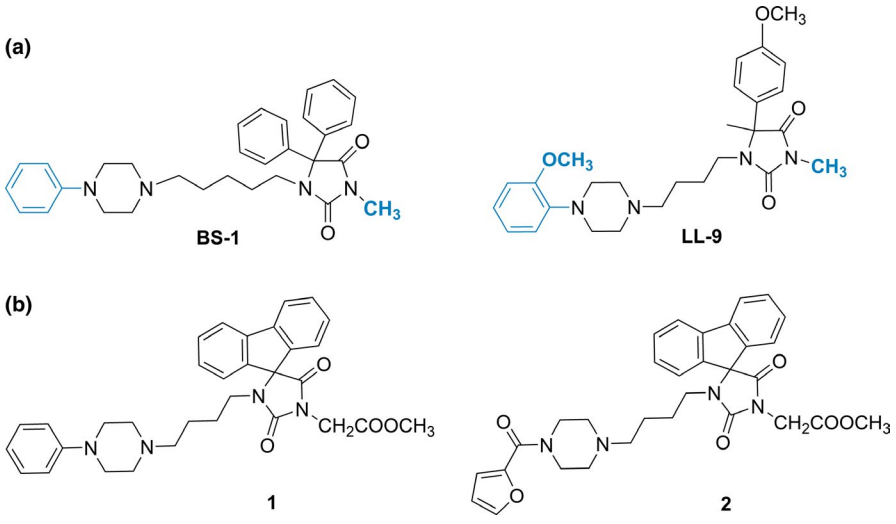


**FIGURE 1** The potent hydantoin efflux pump inhibitors obtained before: (a) the first-generation compounds—**BS-1** and **LL-9** (Spengler et al., 2010) with beneficial substituents denoted in blue; (b) the second-generation fluorene compounds with ester substituent at N3 atom (Żesławska et al., 2016) [Colour figure can be viewed at wileyonlinelibrary.com]

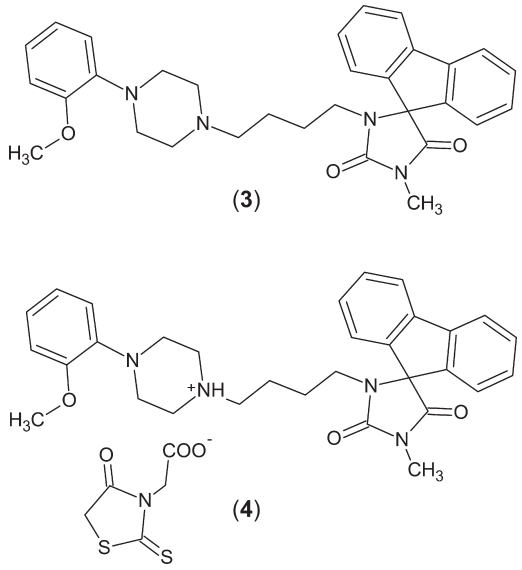


**FIGURE 2** Molecular diagrams of investigated compounds

and 5-spirofluorenehydantoin moieties in order to compare conformations in the current crystal structures to other crystal structures containing these fragments, which were determined earlier.

## 2 | METHODS AND MATERIALS

### 2.1 | Synthesis

Reagents were manufactured by Alfa Aesar (Karlsruhe, Germany) or Sigma-Aldrich (Darmstadt, Germany). Reaction progress was verified using thin layer chromatography (TLC), which was carried out on 0.2 mm Merck silica gel 60 F254 plates. Spots were visualized by UV light. Melting points (mp) were determined using MEL-TEMP II apparatus and are uncorrected. The $^1$H NMR spectra were obtained on a Varian Mercury-VX 300 Mz spectrometer in DMSO-d6. Chemical shifts in $^1$H NMR spectra were reported in parts per million (ppm) on the $\delta$ scale using the solvent signal as an internal standard. Data are reported as follows: chemical shift, multiplicity (s, singlet; br.s., broad singlet; d, doublet; t, triplet; m, multiplet, def., deformed), coupling constant $J$ in Hertz (Hz), number of protons, proton's position (Flu—fluorene, Ar—phenyl at piperazine, Pp—piperazine). IR spectra were recorded on a Jasco FT/IR-410 apparatus using KBr pellets and are reported in cm$^{-1}$. Elemental analyses were within $\pm$0.4% of the theoretical values unless stated otherwise. Synthesis of compound **5** is described elsewhere (Żesławska et al., 2016).

#### 2.1.1 | Synthesis of 1′-methylspiro[fluorene-9,4′-imidazolidine]-2′,5′-dione (6)

Spiro[fluorene-9,4′-imidazolidine]-2′,5′-dione **1** (60 mmol) was dissolved and refluxed in ca. 240 mL of sodium ethanolate. After 15 min, methyl iodide (66 mmol) in 24 mL of absolute ethanol was added to reaction mixture. The mixture was refluxed for 4 hr. After cooling to room temperature, the precipitated product (**2**) was separated and used without further purification. Yellow solid, mp 239°C, yield: 61%, $C_{16}H_{12}N_2O_2$ (MW: 264.28), $R_f(I)$:0.26. $^1$H-NMR [DMSO-d$_6$] $\delta$: 3.01 (s, 3H, $CH_3$), 7.32–7.37 (m, 2H, Ar-2,7-H), 7.46–7.51 (m, 4H, Ar-1,3,6,8-H), 7.88 (d, $J$ = 7.43 Hz, 2H, Ar-4,5-H), 8.87 (s, 1H, NH).

#### 2.1.2 | Synthesis of 3′-(4-bromobutyl)-1′-methylspiro[fluorene-9,4′-imidazolidine]-2′,5′-dione (7)

A mixture of the 1′-methylspiro[fluorene-9,4′-imidazolidine]-2′,5′-dione (30 mmol), TEBA (3.96 mmol) and potassium carbonate (87 mmol) in acetone were stirred for 30 min in room temperature. Then, 1,4-dibromobutane (40 mmol) in acetone was added and the reaction mixture was stirred for 96 hr. Afterward, the inorganic precipitate was filtered off and discarded. The remaining liquor was evaporated and obtained solid was crystallized from absolute ethanol. Creamy solid, mp 126°C, yield: 83%, $C_{20}H_{19}BrN_2O_2$ (MW: 399.28), $R_f(I)$:0.40. $^1$H-NMR (DMSO-d$_6$) $\delta$ (ppm): 1.04 (q, $J$ = 7.40 Hz, 2H, Br–$CH_2$–C$\underline{H}_2$), 1.52 (q, $J$ = 7.00 Hz, 2H, N1–$CH_2$–C$\underline{H}_2$), 2.86 (t, $J$ = 7.00 Hz, 2H, N1–$CH_2$), 3.03 (s, 3H, N3–$CH_3$), 3.20 (t, $J$ = 6.50 Hz, 2H, Br–$CH_2$), 7.31–7.37 ($t_{def}$, 2H, Ar-2,7-H), 7.45–7.53 (m, 4H, Ar-1,3,6,8-H), 7.90–7.93 ($d_{def}$, 2H, Ar-4,5-H).

#### 2.1.3 | Synthesis of 1′-[4-(4-(o-methoxyphenyl)-piperazin-1-yl)butyl]-3′-methyl-spiro(fluoren-9,5′-imid-azolidine)-2′,4′-dione (3)

The commercially available 1-(2-methoxyphenyl)piperazine (5 mmol, 0.96 g), $K_2CO_3$ (2.0 g) and acetone (25 ml) were stirred for 30 min. Then, a solution of 1′-(4-bromo butyl)-3-methyl-spiro(fluorene-9,5′-imidazolidine)-2′,4′-dione **5** (5 mmol, 2.00 g) in acetone (15 ml) was added. The mixture was maintained at reflux for 6 hr, stirred at room temperature for next 15 hr. The precipitate was filtrated off. The filtrate was concentrated to constant weight. The crude residue was purified by crystallization with MeOH to give a yellow precipitate of **3**. Yield 80%; m.p. 135–136°C. Anal. Calcd. for $C_{31}H_{34}N_4O_3$ (**1**): C, 72.92; H, 6.71; N, 10.97; found: C, 72.85; H, 6.77; N, 10.91. $^1$H-NMR (300 MHz, DMSO-d$_6$) $\delta$ (ppm): 0.96–1.06 (q, $J$ = 7.18 Hz, 2H, Pp-$CH_2$–C$\underline{H}_2$), 1.16–1.21 ($q_{def}$, 2H, N1–$CH_2$–C$\underline{H}_2$), 1.93–1.98 (t, $J$ = 7.05 Hz, 2H, Pp-$CH_2$), 2.27 (br.s, 4H, Pp-2,6-H), 2.79 (br.s, 4H, Pp-3,5-H), 2.88–2.92 (t, $J$ = 7.18 Hz, N1–$CH_2$), 3.03 (s, 3H, N–$CH_3$), 3.73 (s, 3H, O–$CH_3$), 6.81–6.92 (m, 4H, Ar–H), 7.32–7.37 ($t_{def}$, 2H,

Flu-2,7-H), 7.47–7.53 ($t_{def}$, 4H, Flu-1,3,6,8-H), 7.90–7.93 ($d_{def}$, 2H, Flu-4,5-H). IR ($cm^{-1}$): 3,451 (N–H), 2,943 (C–H; Ar), 2,814 (C–H; Aliph), 1,768 (C=O; 2), 1,704 (C=O; 4), 1,592 (C=C; Ar).

## 2.2 | Crystallography

Crystals of **3** suitable for X-ray diffraction analysis were obtained from *n*-butyl acetate by slow evaporation of the solvent at room temperature. The **RA** was synthesized according to the three-steps procedure described previously (Tejchman, Skórska-Stania, & Żesławska, 2016). The salt (**4**) of **RA** with **3** was obtained by dissolving both compounds in 1:1 molar ratio in hot propan-2-ol. Crystals appeared after 3 weeks.

Diffraction data for single crystal of **3** were collected at 100 K using the Bruker–Nonius Kappa CCD four circle diffractometer equipped with a Mo (0.71069 Å) *Kα* radiation source. Diffraction data for **4** were collected at 130 K on Oxford Diffraction SuperNova four circle diffractometer, equipped with a Mo (0.71069 Å) *Kα* radiation source, graphite monochromator and Oxford CryoJet system for measurements at low temperature. The phase problem was solved by direct methods using SIR-2014 (Burla et al., 2015). All non-hydrogen atoms were refined anisotropically using weighted full-matrix least-squares on $F^2$. All H atoms bonded to C atoms were placed geometrically in idealized positions and were refined using a riding model. The H atom attached to N2 atom in **4** was identified in difference Fourier. Refinement and further calculations were carried out using SHELXL-2014 (Sheldrick, 2015). For molecular graphics, ORTEP (Farrugia, 2012) and MERCURY (Macrae et al., 2006) programs were used.

Compound **3**: $C_{31}H_{34}N_4O_3$, $M_r = 510.62$, crystal size = $0.45 \times 0.27 \times 0.23$ $mm^3$, triclinic, space group $P\bar{1}$, $a = 10.3380(5)$ Å, $b = 11.4320(5)$ Å, $c = 12.7650(6)$ Å, $\alpha = 92.978(3)°$, $\beta = 111.976(3)°$, $\gamma = 105.089(3)°$, $V = 1331.8(1)$ $Å^3$, $Z = 2$, $T = 100(2)$ K, 10,071 reflections collected, 6,051 unique reflections ($R_{int} = 0.0280$), R1 = 0.0485, wR2 = 0.1246 [$I > 2\sigma(I)$].

Compound **4**: $C_{31}H_{35}N_4O_3^+ \cdot C_5H_4NO_3S_2^-$, $M_r = 701.84$, crystal size = $0.43 \times 0.33 \times 0.03$ $mm^3$, monoclinic, space group $P2_1/c$, $a = 26.3451(4)$ Å, $b = 10.9060(2)$ Å, $c = 12.1116(2)$ Å, $\beta = 100.869(2)°$, $V = 3417.5(1)$ $Å^3$, $Z = 4$, $T = 130(2)$ K, 47,115 reflections collected, 8,237 unique reflections ($R_{int} = 0.0394$), R1 = 0.0421, wR2 = 0.0939 [$I > 2\sigma(I)$].

CCDC 1886047–1886048 contain the supplementary crystallographic data. These data can be obtained free of charge from The Cambridge Crystallographic Data Centre via www.ccdc.cam.ac.uk/data_request/cif.

## 2.3 | Biological assays

### 2.3.1 | Cell lines

The L5178Y mouse T-lymphoma cells (PAR; ECACC Cat. No. 87111908, obtained from FDA, Silver Spring, MD, USA) were transfected with pHa MDR1/A retrovirus, as previously described by Cornwell, Pastan, and Gottesman (1987). The ABCB1-expressing cell line L5178Y (MDR) was selected by culturing the infected cells with colchicine. L5178Y (parent) mouse T-lymphoma cells and the L5178Y human ABCB1 transfected subline were cultured in McCoy's 5A medium (Sigma-Aldrich) supplemented with 10% heat-inactivated horse serum (Sigma-Aldrich), 200 mM L-glutamine (Sigma-Aldrich) and a penicillin streptomycin (Sigma-Aldrich) mixture in concentrations of 100 U/L and 10 mg/L, respectively.

### 2.3.2 | Rhodamine 123 accumulation assay by flow cytometry

The inhibition of ABCB1 by the tested compounds was evaluated using flow cytometry measuring the retention of rhodamine 123 (R123; Sigma-Aldrich) by ABCB1 (P-glycoprotein) in MDR mouse T-lymphoma cells overexpressing the ABCB1 protein. The percentage of mean fluorescence intensity was calculated for the treated MDR cells as compared with the parental (PAR) untreated cells. Verapamil (Sigma-Aldrich) was used as positive control. A fluorescence activity ratio (FAR) was calculated based on the following equation which relates the measured fluorescence values (Żesławska et al., 2016):

$$\mathrm{FAR} = \frac{\mathrm{MDR_{treated}}/\mathrm{MDR_{control}}}{\mathrm{parental_{treated}}/\mathrm{parental_{control}}}.$$

### 2.3.3 | Assay for cytotoxic and antiproliferative effect

The cytotoxicity and antiproliferative assays on T-lymphoma cells were performed according to the protocol described previously (Poljarević et al., 2018; Żesławska et al., 2018). Inhibition of the cell growth was determined according to the formula:

$$100 - \left[\frac{\mathrm{OD_{sample}} - \mathrm{OD_{medium\ control}}}{\mathrm{OD_{cell\ control}} - \mathrm{OD_{medium\ control}}}\right] \times 100.$$

where $IC_{50}$ is defined as the inhibitory dose that reduces the growth of the cells exposed to the compound by 50%. Data represent the $IC_{50}$ mean ($\pm SD$) of three independent experiments.

### 2.3.4 | Checkerboard combination assay

A checkerboard microplate method was applied to study the effect of drug interactions between the tested compounds and the chemotherapeutic drug, doxorubicin (Teva Pharmaceuticals), thus to determine the combination index (CI) for the compounds (Magyari et al., 2018).

On MDR mouse T-lymphoma cells CI values at 50% of the growth inhibition dose ($ED_{50}$), were determined using CompuSyn software (www.combosyn.com; ComboSyn, Inc., Paramus, NJ, USA) to plot four to five data points to each ratio. CI values were calculated by means of the median-effect equation, where CI < 1, CI = 1, or CI > 1 represent synergism, additive effect (or no interaction), or antagonism, respectively (Chou, 2006).

## 3 | RESULTS

### 3.1 | Chemistry

Compound (**3**) was synthesized in four-step synthesis (Figure 3). In the first step (a), spiro(fluoren-9,5′-imidazolidine)-2′,4′-dione (**5**) as a product of Bucherer–Berg condensation of the commercially available 9-fluorenone with ammonium carbonate and potassium cyanide was obtained. Then, *N*-alkylation at position 3 of the hydantoin ring with methyl iodide; (b) was performed (**6**), followed by an alkylation with 1,4-dibromobutane at position 1 that was carried out in acetone with $K_2CO_3$ and TEBA as two-phase mediator; (c). In the last step; (d), the intermediate, 1′-(4-bromobutyl)-3′-methyl-spiro(fluoren-9, 5′-imidazolidine)-2′,4′-dione (**7**), was used for *N*-alkylation of 1-(2-methoxyphenyl)piperazine to give white powder of compound (**3**), after crystallization with ethanol. Details of synthesis of intermediate **5** were described elsewhere (Żesławska et al., 2016).

### 3.2 | Crystallographic studies

Both compounds crystallize with one molecule in the asymmetric unit, but in different space groups **3** in P $\bar{1}$ and **4** in $P2_1/c$. An overview of asymmetric units of **1** and **2** with the atom numbering scheme is shown in Figure 4.

The asymmetric unit of **4** consists of one cation derived by protonation of **3** and one anion derived from **RA**. The protonated N atom is engaged in the charge-assisted $N2^+$–H2···O3a$^-$ hydrogen bond. The spirofluorene substituent is almost perpendicular to hydantoin ring in both structures, the correspondence dihedral angles are 88.19(5)° for **3** and 86.15(5)° for **4**. The conformation of **3** molecule seems to be mainly dependent on the flexible aliphatic chain between piperazine and hydantoin rings. The spacer between hydantoin and piperazine rings consists of four methylene groups and adopts bent conformation at C6 atom. Its conformation is similar in both crystal structures, as indicated by the torsion angles: N1–C6–C7–C8 = 63.85° and 61.76°, C6–C7–C8–C9 = −179.30° and −165.43°, C7–C8–C9–N2 = 169.89° and 170.79° for **3** and **4**, respectively. There is a significant difference in the arrangement of piperazine ring with respect to the linker (Figure 5). The torsion angles C8–C9–N2–C12 and C8–C9–N2–C10 differ in both structures, namely, these values are 69.23° and −169.11° for **3** and −78.13° and 48.62° for **4**. The piperazine ring adopts chair conformation in both structures. The mutual orientation of piperazine and aromatic rings is similar. The corresponding dihedral angle is 51.25(7)° and 46.41(7)° for **3** and **4**, respectively.

The packing of molecules in the crystal structure of **3** is dominated by C–H···O intermolecular interactions. The

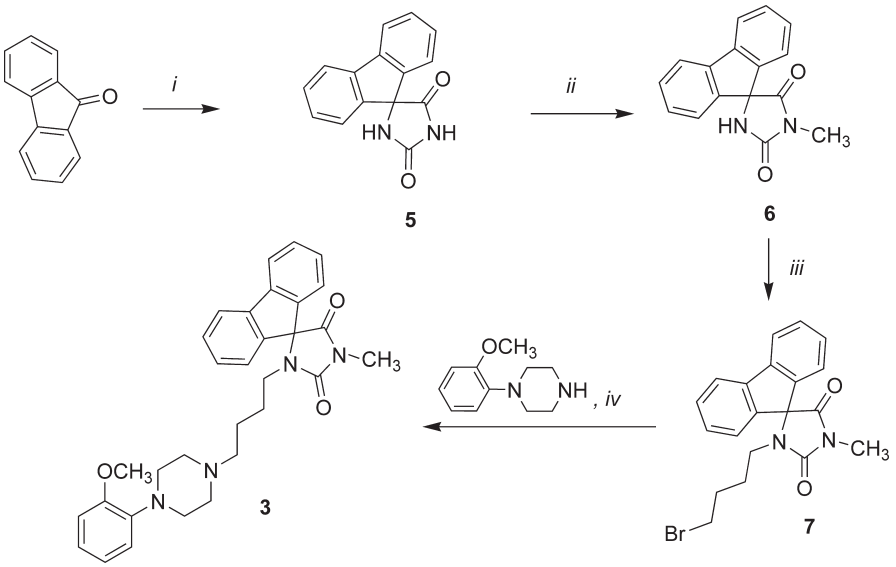


**FIGURE 3** The synthesis route. Conditions: (i) KCN, $(NH_4)_2CO_3$, 50% EtOH, 48 hr, 560°C; (ii) $CH_3I$, EtONa, reflux for 3 hr; (iii) 1,4-dibromobutane, $K_2CO_3$, TEBA, acetone, stirring at rt for 96 hr; (iv) $K_2CO_3$, acetone, reflux for 5 hr

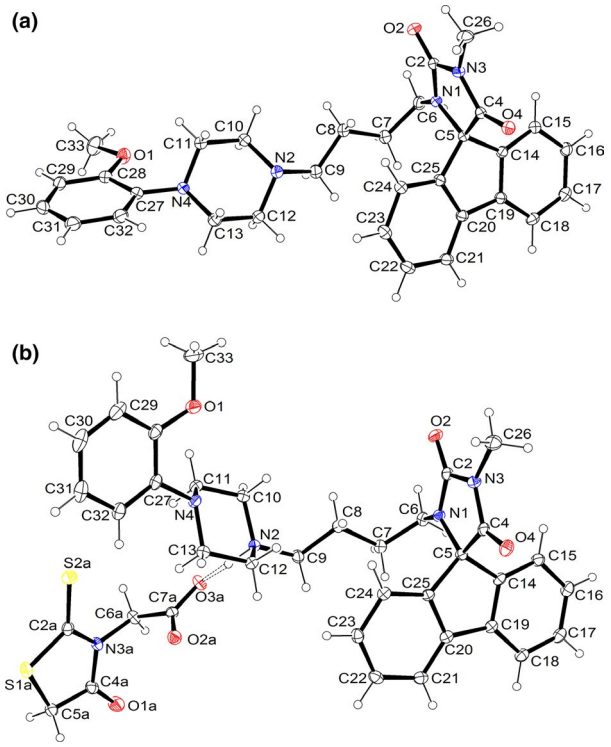


**FIGURE 4** The molecular structures of (a) **3** and (b) **4** showing the atom numbering scheme. Displacement ellipsoids are drawn at the 30% probability level. Dashed line indicates hydrogen bond [Colour figure can be viewed at wileyonlinelibrary.com]

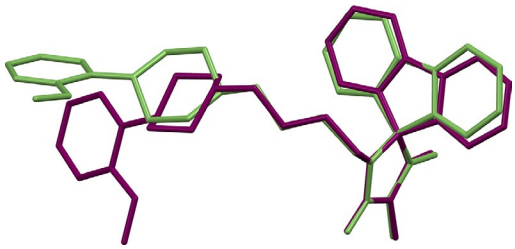

**FIGURE 5** The overlap of the hydantoin rings in the crystal structure of **3** green and **4** purple. The hydrogen atoms have been omitted for clarity [Colour figure can be viewed at wileyonlinelibrary.com]

parameters of these interactions are listed in Table 1. Only oxygen atoms of hydantoin ring are engaged in intermolecular interactions. The spirofluorene substituent of two molecules, related by inversion centre, is engaged in π-π interactions.

In the crystal structure of **4** different arrangements of the cations in comparison with **3** is observed. In this case, there are not observed the $\pi$–$\pi$ interactions between spirofluorene substituents. The crystal lattice is dominated by $N^+$–H···$O^-$, C–H···N, C–H···O and C–H···S intermolecular interactions. Parameters of these interactions are presented in Table 2. It is worth noting that **RA** anion is involved in many hydrogen bonds, both as an acceptor with the use of oxygen and sulfur atoms, and as a donor hydrogen atoms by methylene group.

### 3.3 | Biological activities

Arylpiperazine derivatives of 5-spirofluorenehydantoin showed the capacity to inhibit an MDR efflux pump such as the ABCB1 (Żesławska et al., 2016). In Table 3, there are presented the biological activity results of **3**, **RA** and the salt **4**. These compounds were investigated toward their efflux modulating, cytotoxic, antiproliferative and combination effects in sensitive and resistant mouse T-lymphoma cells.

Compound **3** displayed efflux modulating effect, as well as the cytotoxic and antiproliferative effects in both cell lines. However, **RA** showed only weak antiproliferative effect in MDR cells. The investigated salt **4** possessed similar activity as active compound **3** in the case of efflux modulating and antiproliferative effects, while the cytotoxic activity was twice reduced. In the combination assay, compounds **3** and **4** showed strong synergistic effect with doxorubicin (Table 4).

## 4 | DISCUSSION

The molecular structures of **3** and **4** were compared to other molecules containing 5-spirofluorenehydantoin moiety with determined crystal structures. The arrangement of this fragment is similar to other 5-spirofluorenehydantoin derivatives, in which the values of the angle between the planes of hydantoin and spirofluorene moieties are 86.7°, 89.7° (Żesławska et al., 2016). There is also determined the crystal structure of 5-spirofluorenehydantoin, in which this angle is 87.0° (Todorov, Nikolova, Naydenova, & Shivachev, 2012).

We have also analyzed the mutual orientation of piperazine and aromatic rings in other crystal structures. We have done a search of the Cambridge Structure Database (CSD, Version 5.39) (Groom et al., 2016) for crystal structures containing o-methoxyphenyl substituent at nitrogen atom of piperazine ring in order to see the values of the angle between the planes of piperazine and aromatic rings. As shown in Figure 6 for 43 hits of organic compounds, the vast majority have value of this angle in the range from 39° to 48°. This orientation is related to the presence of metoxy group in *ortho* position. The oxygen atom of this group is engaged in a weak intramolecular interaction with the equatorial hydrogen atom of the piperazine ring. The obtained value of this angle for **4** is very frequent observed in other crystal structures containing 2-methoxyphenylpiperazine moiety deposited in the CSD, while the value for **3** is less frequent.

We compared obtained biological results with the results of other two spirofluorenehydantoin derivatives (**1** and **2**) possessing determined crystal structures and evaluated

**TABLE 1** Intermolecular hydrogen-bonds geometry for **3**

| D–H···A | H···A (Å) | D···A (Å) | D–H–A (°) | Symmetry code |
|---|---|---|---|---|
| C15–H15···O2 | 2.50 | 3.427 (2) | 167 | $-x + 1, -y + 1, -z + 2$ |
| C18–H18···O4 | 2.73 | 3.377 (2) | 126 | $-x + 1, -y + 1, -z + 1$ |
| C23–H23···O4 | 2.51 | 3.348 (2) | 148 | $-x, -y + 1, -z + 1$ |
| C29–H29···O2 | 2.49 | 3.418 (2) | 167 | $-x, -y + 2, -z + 2$ |

**TABLE 2** Intermolecular hydrogen-bonds geometry for **4**

| D–H···A | H···A (Å) | D···A (Å) | D–H–A (°) | Symmetry code |
|---|---|---|---|---|
| N2–H2···O3A | 1.58 | 2.545 (2) | 172 | |
| C5A–H5A···O2 | 2.29 | 3.150 (2) | 145 | $x, -y + 3/2, z + 1/2$ |
| C5A–H5B···N4 | 2.36 | 3.325 (2) | 164 | $x, y + 1, z$ |
| C6–H6A···O4 | 2.44 | 3.318 (2) | 148 | $x, -y + 1/2, z + 1/2$ |
| C10–H10B···S1A | 2.88 | 3.530 (2) | 124 | $x, -y + 3/2, z + 1/2$ |
| C13–H13A···O2A | 2.62 | 3.424 (2) | 138 | |
| C13–H13B···O2A | 2.52 | 3.426 (2) | 153 | $x, -y + 3/2, z + 1/2$ |
| C26–H26A···O2A | 2.53 | 3.316 (2) | 137 | $x, y - 1, z$ |

**TABLE 3** The efflux modulating, cytotoxic, and antiproliferative effects of **3**, **4** and rhodanine-3-acetic acid (**RA**) on L5178Y sensitive (parental [PAR]) and resistant (MDR) mouse T-lymphoma cells

| | FAR[a] | | $IC_{50}$ (μM) | | | |
|---|---|---|---|---|---|---|
| | Concentration (μM) | | Cytotoxic effect | | Antiproliferative effect | |
| Cpd | 2 | 20 | PAR | MDR | PAR | MDR |
| **3** | 7.22 | 75.83 | 19.40 ± 0.13 | 13.25 ± 0.55 | 11.56 ± 0.59 | 6.98 ± 0.11 |
| **4** | 6.35 | 73.28 | 40.46 ± 1.08 | 28.26 ± 1.16 | 9.83 ± 0.78 | 7.05 ± 0.16 |
| **RA** | 0.81 | 0.75 | >100 | >100 | >100 | 41.14 ± 1.20 |

*Notes*. Verapamil (20 μM) fluorescence activity ratio (FAR) = 4.81, DMSO (2%) FAR = 0.92.
[a]FAR values are calculated for the MDR mouse T-lymphoma cell line.

P-glycoprotein inhibition properties and cytotoxic effects (Żesławska et al., 2016). The biological activities results are listed in Table 5. These compounds differ in substituents at N3 and N4 atoms in comparison with **3**. Both compounds (**1** and **2**) were less potent than **3** and **4**, displaying up to four-fold stronger P-gp-inhibitory action than that of verapamil, whereas more than 15-fold of the action of verapamil was demonstrated by **3** and **4** in the corresponding concentration. The cytotoxic effect of **1** and **2** was also distinctly weaker in comparison with **3** and **4**.

In Figure 7a, it is presented the overlap of hydantoin rings in **1**, **2**, **3** and **4** in order to see the changes in conformation of the same moiety in these molecules. A common part of these compounds is 1′-[4-(piperazin-1-yl)butyl]-spiro(fluoren-9,5′-imidazolidine-2′,4′-dione fragment. The mutual orientation of spirofluorene and hydantoin moiety is the same in all molecules. Differences are visible in the conformation of aliphatic chain, which consequently changes the distances of the piperazine ring from hydantoin and aromatic ring. These differences are characterized by the values of torsion angles C2–N1–C6–C7: −99.11°, 124.72°, −120.82° and −125.67°, as well as N1–C6–C7–C8: 54.54°, −169.29°, 61.72° and 63.96° for **1**, **2**, **3** and **4**, respectively. For compound **2**, the values of compared torsion angles differ significantly in comparison with other three. These conformational changes cause a different spatial distribution of N4-substituted piperazine ring with respect to the 5-spirofluorenehydantoin system. Moreover, in Figure 7b, it is presented the superposition of all four compared structures with respect to aliphatic chain in order to see the mutual spatial orientation of 5-spirofluorenehydantoin moiety and N4-substituted piperazine ring. Only for compound **2**, the spirofluorene system is perpendicular to aliphatic chain, while for other three compounds is parallel.

It can be concluded that the presence of not active compound **RA** did not influence significantly on biological activities toward efflux modulating and antiproliferative effects of **3**, and therefore, a partial change of conformation of *N*-(o-methoxyphenyl)-piperazine moiety in molecule **4** is not related to these activities. In contrast, a distinct influence of **RA** on the cytotoxic effects was observed. The bending and twisting of piperazine ring in relation to the linker seem to be not favorable for the cytotoxic activity.

It was postulated earlier that the presence of an aromatic ring in compound is important for cancer efflux pumps

**TABLE 4** Type of interaction between compounds and doxorubicin on multidrug-resistant (MDR) T-lymphoma cells

| Compound | Ratio[a] | CI at $ED_{50}$[b] | Interaction |
|---|---|---|---|
| **3** | 11.6:1 | 0.12 ± 0.1 | Strong synergism |
| **4** | 13.9:1 | 0.18 ± 0.1 | Strong synergism |

[a]Data are shown as the best combination ratio between the tested compounds and doxorubicin. [b]Combination index (CI) values at the 50% growth inhibition dose ($ED_{50}$) were determined by the CompuSyn software to plot four to five data points at each ratio. CI values were calculated by means of the median-effect equation, where CI: 0.1–0.3 represent strong synergism.

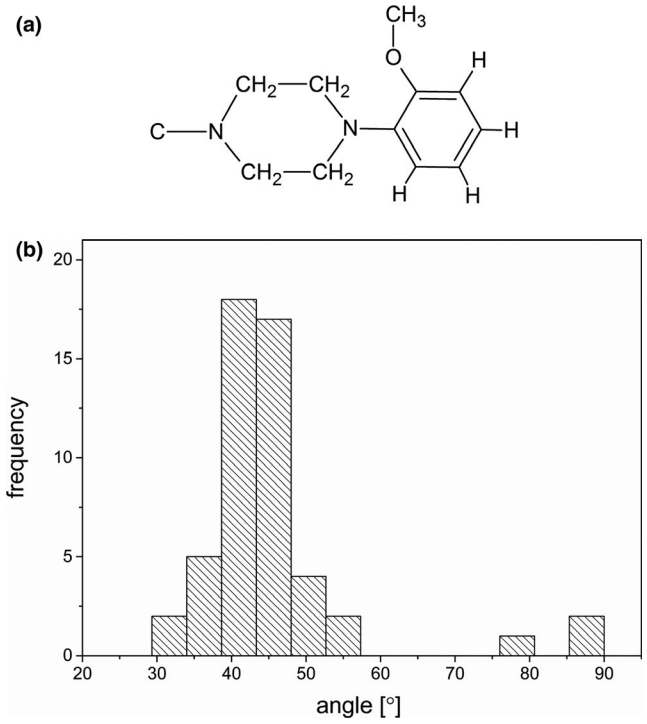


**FIGURE 6** (a) The fragment used in the search of the Cambridge Structural Database (CSD). (b) The distribution of angles between the plane containing of four C atoms of piperazine ring and the plane of aromatic ring for 43 hits found in the CSD containing 2-methoxyphenylpiperazine fragment

modulator properties, while the presence of second aromatic ring increased inhibition of this efflux pump (Handzlik et al., 2012; Reis et al., 2013). The influence of other pharmacophore features, namely, positive ionizable center and hydrogen bond acceptor, is not very strong on this activity, but is profitable (Handzlik et al., 2012).

Taking this into consideration, we analyzed the distances between aromatic rings and nitrogen atoms in these compounds (Table 6). We have chosen the following distances: between the centroids of aromatic rings ($C_g1$, $C_g2$—aromatic rings in spirofluorene substituent, $C_g3$—aromatic ring at N4 of piperazine ring), between the centroids of aromatic rings and nitrogen atoms (N2 and N4), as well as between nitrogen atoms (N1, N2 and N4).

**TABLE 5** Efflux modulating and cytotoxic effects of the compounds **3** and **4** on L5178Y sensitive (parental [PAR]) and resistant (MDR) mouse T-lymphoma cells (Żesławska et al., 2016)

| | FAR[a] | | $IC_{50}$ (μM) | |
|---|---|---|---|---|
| | Concentration (μM) | | Cytotoxic effect | |
| Cpd | 2 | 20 | PAR | MDR |
| **1** | 21.61 | 70.19 | 53 ± 5 | >100 |
| **2** | 1.86 | 24.89 | 59 ± 13 | 63 ± 9 |

*Notes*. Verapamil (20 μM) fluorescence activity ratio (FAR) = 17.59, DMSO (2%) FAR = 0.84.
[a]FAR values are calculated for the MDR mouse T-lymphoma cell line.

All compounds were more active than verapamil, but the most active **3** is 10-fold higher active than **2**. Only for compound **2**, the extended conformation of linker is observed, which increases the distance between N1 and N2, as well as N1 and N4 in comparison with **1**, **3** and **4**. Likewise, the increased distances between centroid ($C_g2$) and nitrogen atoms (N2, N4) are observed, while the distances between centroid (Cg1) and N2 and N4 atoms decreased. Although the extended conformation of the linker seems to be responsible for weaker cancer efflux pumps activity, probably it is not only one factor because this compound possesses an

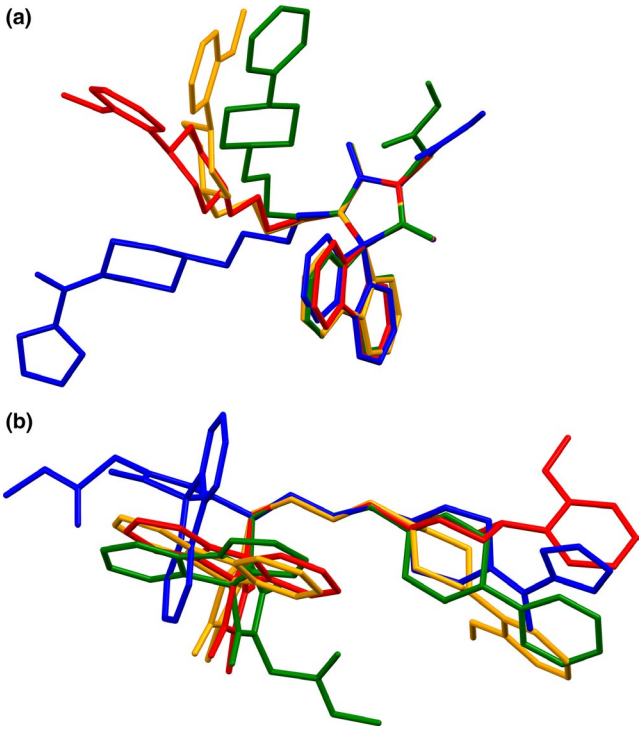


**FIGURE 7** The overlap of (a) the hydantoin rings and (b) the aliphatic chains (C6, C7, C8 and C9 atoms) in the crystal structures of **1**—green, **2**—blue, **3**—red, and **4**—yellow. The hydrogen atoms have been omitted for clarity [Colour figure can be viewed at wileyonlinelibrary.com]

**TABLE 6** Comparison of the selected distances (Å) in the crystal structures of **1**, **2**, **3** and **4**

| | $C_g1\cdots C_g3$ | $C_g2\cdots C_g3$ | $C_g1\cdots N2$ | $C_g2\cdots N2$ | $C_g1\cdots N4$ | $C_g2\cdots N4$ | N1···N2 | N1···N4 |
|---|---|---|---|---|---|---|---|---|
| **1** | 13.17 | 10.01 | 8.40 | 5.60 | 10.57 | 7.35 | 5.10 | 7.35 |
| **2** | – | – | 7.33 | 7.19 | 9.86 | 9.69 | 6.24 | 8.94 |
| **3** | 13.47 | 9.90 | 7.86 | 4.77 | 10.69 | 7.29 | 5.25 | 8.04 |
| **4** | 12.82 | 9.41 | 8.23 | 5.25 | 10.28 | 6.99 | 5.45 | 7.10 |

acyl-heterocyclic ring, in place of desirable aromatic one, at piperazine moiety.

## 5 | CONCLUSIONS

The studies performed allowed to find a new very potent cancer efflux pump inhibitor (**3**) that represents 3-methyl derivatives of spiro(fluoren-9,5′-imidazolidine)-2′,4′-dione. The compound **3** can also be considered as potential anticancer agent, useful against drug-resistant cells, since the cytotoxic and antiproliferative properties of **3** on T-lymphoma were significant, and even more potent in the case of MDR cells if comparing to the PAR ones. Furthermore, our results indicated that compound **3** converted into salt of inactive **RA** (**4**) has maintained both, the efflux pump inhibitory and antiproliferative, activities. In particular, both forms (**3** and **4**) had a strong synergistic action with doxorubicin, used as a reference anticancer agent. So far, we have not enough crystal structures of active aromatic hydantoin derivatives to uniquely determine the preferred conformation and distances between the pharmacophoric features responsible for their cancer efflux pump inhibition. However, this comprehensive study significantly contributed to extend knowledge in this field and can be useful for further considerations.

## ACKNOWLEDGMENTS

The work was partly supported by Pedagogical University of Cracow (BS-465/G/2018) and by Polish Statutory Research Project K/ZDS/007886.

## CONFLICT OF INTEREST

The authors declare no conflict of interest.

## ORCID

*Ewa Żesławska* https://orcid.org/0000-0003-1946-9370

## REFERENCES

Burla, M. C., Caliandro, R., Carrozzini, B., Cascarano, G. L., Cuocci, C., Giacovazzo, C., … Polidori, G. (2015). Crystal structure determination and refinement *via* SIR2014. *Journal of Applied Crystallography*, *48*, 306–309. https://doi.org/10.1107/S1600576715001132

Carmi, C., Cavazzoni, A., Zuliani, V., Lodola, A., Bordi, F., Plazzi, P. V., … Mor, M. (2006). 5-Benzylidene-hydantoins as new EGFR inhibitors with antiproliferative activity. *Bioorganic and Medicinal Chemistry Letters*, *16*, 4021–4025. https://doi.org/10.1016/j.bmcl.2006.05.010

Cavazzoni, A., Alfieri, R. R., Carmi, C., Zuliani, V., Galetti, M., Fumarola, C., … Petronini, P. G. (2008). Dual mechanisms of action of the 5-benzylidene-hydantoin UPR1024 on lung cancer cell lines. *Molecular Cancer Therapeutics*, *7*, 361–370. https://doi.org/10.1158/1535-7163.MCT-07-0477

Chou, T. C. (2006). Theoretical basis, experimental design, and computerized simulation of synergism and antagonism in drug combination studies. *Pharmacological Reviews*, *58*, 621–681. https://doi.org/10.1124/pr.58.3.10

Cornwell, M. M., Pastan, I., & Gottesman, M. M. (1987). Certain calcium channel blockers bind specifically to multidrug-resistant human KB carcinoma membrane vesicles and inhibit drug binding to P-glycoprotein. *Journal of Biological Chemistry*, *262*, 2166–2170.

Farrugia, L. J. (2012). WinGX and ORTEP for Windows: An update. *Journal of Applied Crystallography*, *45*, 849–854. https://doi.org/10.1107/S0021889812029111

Groom, C. R., Bruno, I. J., Lightfoot, M. P., & Ward, S. C. (2016). The Cambridge structural database. *Acta Crystallographica Section C Structural Chemistry*, *B72*, 171–179.

Handzlik, J., Maciąg, D., Kubacka, M., Mogilski, S., Filipek, B., Stadnicka, K., & Kieć-Kononowicz, K. (2008). Synthesis, alpha 1-adrenoceptor antagonist activity and SAR study of novel arylpiperazine derivatives of phenytoin. *Bioorganic and Medicinal Chemistry*, *16*, 5982–5998. https://doi.org/10.1016/j.bmc.2008.04.058

Handzlik, J., Spengler, G., Mastek, B., Dela, A., Molnar, J., Amaral, L., & Kieć-Konowicz, K. (2012). 5-Arylidene(thio)hydantoin derivatives as modulators of cancer efflux pump. *Acta Poloniae Pharmaceutica. Drug Research*, *69*(1), 149–153.

Handzlik, J., Szymańska, E., Nędza, K., Kubacka, M., Siwek, A., Mogilski, S., … Kieć-Kononowicz, K. (2011). Pharmacophore models based studies on the affinity and selectivity toward 5-HT1A with reference to α1-adrenergic receptors among arylpiperazine derivatives of phenytoin. *Bioorganic and Medicinal Chemistry*, *19*, 1349–1360. https://doi.org/10.1016/j.bmc.2010.11.051

Khanfar, M. A., & El Sayed, K. A. (2010). Phenylmethylene hydantoins as prostate cancer invasion and migration inhibitors. CoMFA approach and QSAR analysis. *European Journal of Medicinal Chemistry*, *45*, 5397–5405. https://doi.org/10.1016/j.ejmech.2010.08.066

Macrae, C. F., Edgington, P. R., McCabe, P., Pidcock, E., Shields, G. P., Taylor, R., … van de Streek, J. (2006). Mercury: Visualization and

analysis of crystal structures. *Journal of Applied Crystallography*, *39*, 453–457. https://doi.org/10.1107/S002188980600731X

Magyari, J., Holló, B. B., Vojinović-Ješić, S. L., Radanović, M. M., Armaković, S., Armaković, J. S., … Szécsényi, M. K. (2018). Interactions of Chiff base compounds and their coordination complexes with the drug cisplatin. *New Journal of Chemistry*, *42*, 5834–5843. https://doi.org/10.1039/C8NJ00357B

Poljarević, J. M., Tamás, G. G., May, N. V., Spengler, G., Dömötör, O., Savić, A. R., … Enyedy, É. A. (2018). Comparative solution equilibrium and structural studies of half-sandwich ruthenium(II)($\eta^6$-toluene) complexes of picolinate derivatives. *Journal of Inorganic Biochemistry*, *181*, 74–85. https://doi.org/10.1016/j.jinorgbio.2017.12.017

Raynaud, J. P., Bonne, C., Bouton, M. M., Lagace, L., & Labrie, F. (1979). Steroid hormone receptors and pharmacology. *Journal of Steroid Biochemistry*, *11*, 93–99. https://doi.org/10.1016/0022-4731(79)90281-4

Raynaud, J. P., Bonne, C., Moguilewsky, M., Lefebvre, F. A., Belanger, A., & Labrie, F. (1984). The pure antiandrogen ru 23908 (anandron®), a candidate of choice for the combined antihormonal treatment of prostatic cancer: A review. *Prostate*, *5*, 299–311. https://doi.org/10.1002/(ISSN)1097-0045

Reis, M., Ferreira, R. J., Santos, M. M., Dos Santos, D. J. V., Molnar, J., & Ferreira, M. J. U. (2013). Enhancing macrocyclic diterpenes as multidrug-resistance reversers: Structure-activity studies in jolkinol D derivatives. *Journal of Medicinal Chemistry*, *56*, 748–760. https://doi.org/10.1021/jm301441w

Sheldrick, G. M. (2015). Crystal structure refinement with SHELXL. *Acta Crystallographica Section C Structural Chemistry*, *C71*, 3–8. https://doi.org/10.1107/S2053229614024218

Spengler, G., Evaristo, M., Handzlik, J., Serly, J., Molnár, J., Viveiros, M., … Amaral, L. (2010). Biological activity of hydantoin derivatives on P-glycoprotein (ABCB1) of mouse lymphoma cells. *Anticancer Research*, *30*, 4867–4871.

Spengler, G., Handzlik, J., Ocsovszki, I., Viveiros, M., Kieć-Kononowicz, K., Molnar, J., & Amaral, L. (2011). Modulation of multidrug efflux pump activity by new hydantoin derivatives on colon adenocarcinoma cells without inducing apoptosis. *Anticancer Research*, *31*, 3285–3288.

Szymańska, E., & Kieć-Kononowicz, K. (2002). Antimycobacterial activity of 5-arylidene aromatic derivatives of hydantoin. *Farmaco*, *57*, 355–362. https://doi.org/10.1016/S0014-827X(01)01194-6

Szymańska, E., Kieć-Kononowicz, K., Białecka, A., & Kasprowicz, A. (2002). Antimicrobial activity of 5-arylidene aromatic derivatives of hydantoin. Part 2. *Farmaco*, *57*, 39–44. https://doi.org/10.1016/S0014-827X(01)01172-7

Tejchman, W., Skórska-Stania, A., & Żesławska, E. (2016). The crystal structures of three rhodanine-3-carboxylic acids. *Journal of Chemical Crystallography*, *46*, 181–187. https://doi.org/10.1007/s10870-016-0644-0

Todorov, P. T., Nikolova, R. P., Naydenova, E. D., & Shivachev, B. L. (2012). Synthesis and structural characterization of spiro(fluorene-9,4′-imidazolidine)-2′,5′-dione and (9H-fluorene-9-yl)urea. *Journal of Chemical Crystallography*, *42*, 566–572. https://doi.org/10.1007/s10870-012-0280-2

Żesławska, E., Jacob, U., Sturzebecher, J., & Oleksyn, B. J. (2006). The crystal structures of 3-TAPAP in complexes with the urokinase-type plasminogen activator and picrate. *Bioorganic and Medicinal Chemistry Letters*, *16*, 228–234. https://doi.org/10.1016/j.bmcl.2005.08.089

Żesławska, E., Kincses, A., Spengler, G., Nitek, W., Wyrzuc, K., Kieć-Kononowicz, K., & Handzlik, J. (2016). The 5-aromatic hydantoin-3-acetate derivatives as inhibitors of the tumour multidrug resistance efflux pump P-glycoprotein (ABCB1): Synthesis, crystallographic and biological studies. *Bioorganic and Medicinal Chemistry*, *24*, 2815–2822. https://doi.org/10.1016/j.bmc.2016.04.055

Żesławska, E., Kincses, A., Unger, V., Tóth, V., Spengler, G., Nitek, W., & Tejchman, W. (2018). Exocyclic sulfur and selenoorganic compounds towards their anticancer effects: Crystallographic and biological studies. *Anticancer Research*, *38*, 4577–4584. https://doi.org/10.21873/anticanres.12762

Żesławska, E., Nitek, W., & Handzlik, J. (2017). Conformational study of (Z)-5-(4-chlorobenzylidene)-2-[4-(2-hydroxyethyl)piperazin-1-yl]-3*H*-imidazol-4(5*H*)-one in different environments: Insight into the structural properties of bacterial efflux pump inhibitors. *Acta Crystallographica Section C Structural Chemistry*, *C73*, 1151–1157. https://doi.org/10.1107/S2053229617016461

Żesławska, E., Nitek, W., Marona, H., & Waszkielewicz, A. W. (2018). Supramolecular architectures of succinates of 1-hydroxypropan-2-aminium derivatives. *Acta Crystallographica Section C Structural Chemistry*, *C73*, 856–862. https://doi.org/10.1107/S2053229618008574

Żesławska, E., Oleksyn, B. J., Fabre, A., & Benoit-Vical, F. (2014). Influence of amodiaquine on the antimalarial activity of ellagic acid: Crystallographic and biological studies. *Chemical Biology and Drug Design*, *84*, 669–675. https://doi.org/10.1111/cbdd.12359

Żesławska, E., Oleksyn, B. J., & Stadnicka, K. (2003). Amiloride conformation: The effect of different crystalline environments. *Structural Chemistry*, *15*, 567–572. https://doi.org/10.1007/s11224-004-0731-2

Żesławska, E., Sturzebecher, J., & Oleksyn, B. J. (2007). Geometry of GPPE binding to picrate and to the urokinase type plasminogen activator. *Bioorganic and Medicinal Chemistry Letters*, *17*, 6212–6215. https://doi.org/10.1016/j.bmcl.2007.09.020

**How to cite this article:** Żesławska E, Kincses A, Spengler G, Nitek W, Tejchman W, Handzlik J. Pharmacophoric features for a very potent 5-spirofluorenehydantoin inhibitor of cancer efflux pump ABCB1, based on X-ray analysis. *Chem Biol Drug Des*. 2019;93:844–853. https://doi.org/10.1111/cbdd.13473